Magnetic Resonance Imaging 46 (2018) 98–105

Contents lists available at ScienceDirect

Magnetic Resonance Imaging

journal homepage: www.elsevier.com/locate/mri

Original contribution

Evaluation of dynamic contrast-enhanced MRI biomarkers for stratified cancer medicine: How do permeability and perfusion vary between human tumours?

Ross A. Little[a], Hervé Barjat[b], Jennifer I. Hare[c], Mary Jenner[b], Yvonne Watson[a], Susan Cheung[a], Katherine Holliday[a], Weijuan Zhang[a], James P.B. O'Connor[d], Simon T. Barry[c], Sanyogitta Puri[e], Geoffrey J.M. Parker[a,f], John C. Waterton[a,b,f,*]

[a] Centre for Imaging Sciences, Division of Informatics Imaging & Data Sciences, School of Health Sciences, Faculty of Biology Medicine & Health, University of Manchester, Manchester Academic Health Sciences Centre, Manchester M13 9PL, UK
[b] Formerly AstraZeneca, Alderley Park, Macclesfield, Cheshire SK10 4TG, UK
[c] IMED Oncology, AstraZeneca, Li Ka Shing Centre, Cambridge CB2 0RE, UK
[d] Division of Cancer Sciences, Faculty of Biology Medicine & Health, University of Manchester, Manchester Academic Health Sciences Centre, Oxford Road, Manchester M13 9PL, UK
[e] AstraZeneca, Alderley Park, Macclesfield, Cheshire SK10 4TG, UK
[f] Bioxydyn Ltd., Rutherford House, Manchester M15 6SZ, UK

ARTICLE INFO

Keywords:
Drug delivery
Dynamic contrast-enhanced MRI
Enhanced permeability and retention
Imaging biomarkers
Personalised medicine
Solid tumours

ABSTRACT

Background: Solid tumours exhibit enhanced vessel permeability and fenestrated endothelium to varying degree, but it is unknown how this varies in patients between and within tumour types. Dynamic contrast-enhanced (DCE) MRI provides a measure of perfusion and permeability, the transfer constant K^{trans}, which could be employed for such comparisons in patients.

Aim: To test the hypothesis that different tumour types exhibit systematically different K^{trans}.

Materials and methods: DCE-MRI data were retrieved from 342 solid tumours in 230 patients. These data were from 18 previous studies, each of which had had a different analysis protocol. All data were reanalysed using a standardised workflow using an extended Tofts model. A model of the posterior density of median K^{trans} was built assuming a log-normal distribution and fitting a simple Bayesian hierarchical model.

Results: 12 histological tumour types were included. In glioma, median K^{trans} was 0.016 min^{-1} and for non-glioma tumours, median K^{trans} ranged from 0.10 (cervical) to 0.21 min^{-1} (prostate metastatic to bone). The geometric mean (95% CI) across all the non-glioma tumours was 0.15 (0.05, 0.45) min^{-1}. There was insufficient separation between the posterior densities to be able to predict the K^{trans} value of a tumour given the tumour type, except that the median K^{trans} for gliomas was below 0.05 min^{-1} with 80% probability, and median K^{trans} measurements for the remaining tumour types were between 0.05 and 0.4 min^{-1} with 80% probability.

Conclusion: With the exception of glioma, our hypothesis that different tumour types exhibit different K^{trans} was not supported. Studies in which tumour permeability is believed to affect outcome should not simply seek tumour types thought to exhibit high permeability. Instead, K^{trans} is an idiopathic parameter, and, where permeability is important, K^{trans} should be measured in each tumour to personalise that treatment.

1. Introduction

Personalised medicine creates an enhanced role for imaging biomarkers [1]. In oncology, for example, some patients fail to benefit from medical treatment simply because the drug fails to reach its site of action. Imaging biomarkers may identify patients whose tumours are accessible to drug treatment. Such imaging biomarkers would be of broad interest. Drug developers may prefer trials of such drugs to be

* Corresponding author at: University of Manchester, Stopford Building, Oxford Road, Manchester M13 9PL, UK.
E-mail addresses: ross.little@manchester.ac.uk (R.A. Little), herve.barjat@stfc.ac.uk (H. Barjat), Jennifer.Hare@astrazeneca.com (J.I. Hare), Yvonne.Watson-2@manchester.ac.uk (Y. Watson), Susan.Cheung@manchester.ac.uk (S. Cheung), kholliday@mcrc.man.ac.uk (K. Holliday), weijuan.zhang@merck.com (W. Zhang), James.O'Connor@manchester.ac.uk (J.P.B. O'Connor), Simon.T.Barry@astrazeneca.com (S.T. Barry), Sanyogitta.Puri@astrazeneca.com (S. Puri), geoff.parker@manchester.ac.uk (G.J.M. Parker), john.waterton@manchester.ac.uk (J.C. Waterton).

https://doi.org/10.1016/j.mri.2017.11.008
Received 12 July 2017; Received in revised form 8 November 2017; Accepted 13 November 2017

stratified by tumour permeability so as to identify the groups most likely to benefit. Regulatory authorities may demand a predictive biomarker to contraindicate drug in patients with low tumour permeability who are least likely to benefit. Oncologists want to personalise treatment by selecting drugs most likely to reach their target and benefit patients: radiologists want to identify those patients.

A systemic drug normally arrives in the tumour via the vasculature, but to reach its target on a neoplastic cell, it must first traverse the vascular endothelium. Enhanced perfusion and vascular permeability in tumours are expected to accelerate the arrival of a drug at its target and may enhance retention of macromolecules [2,3]. This enhanced permeability and retention effect is viewed as a universal property of solid tumours [4], but the lack of comparative data assessing tumour perfusion and permeability in human subjects has hindered the evaluation of its clinical relevance for different classes of therapies [5]. The effect is likely to be more variable and complex in humans than in mouse models [6,7]: one imaging study showed therapeutic liposome accumulation to vary between 5% and 30% of the injected dose per weight of tumour [8]. Such heterogeneity has clinical implications: patients and tumours with high levels of drug accumulation may receive therapeutic benefit, while patients with low accumulation will only experience off-target adverse effects.

Dynamic contrast-enhanced (DCE)-MRI and DCE-CT rely on enhanced tumour uptake of contrast agents, reflecting enhanced perfusion and permeability. However, while radiologists commonly observe that particular tumours are 'highly enhancing', they do not routinely quantify their visual impression in a way that allows precise between-patient and between-centre comparisons. DCE-MRI and -CT also allow calculation of the transfer constant K^{trans}, which quantifies the permeability-surface area [9]. K^{trans} and related metrics have been successfully employed as pharmacodynamic biomarkers in over 100 clinical studies of anti-vascular agents as well as numerous studies of tumour biology [10] in different studies and centres [10,11]. However, few studies included > 40 patients [12], and the DCE-MRI biomarkers were not generally measured in a consistent or standard way. While change in K^{trans} can be compared between studies [13], baseline values cannot. This lack of standardisation poses a significant impediment [14], preventing objective comparison of permeability-driven enhancement of different tumour types. There is therefore a need for larger analyses to evaluate the pre-treatment parameters for stratifying tumour permeability.

In planning the development of an investigational new cancer medicine, it is important to select the tumour types most likely to respond. Our hypothesis was that tumour types exhibit systematic differences in permeability and perfusion, and consequently in K^{trans}. The null hypothesis was therefore that K^{trans} is an idiopathic parameter that must be individually measured in each patient and each tumour. To test our hypothesis, a standardised analysis of tumour K^{trans} was performed in 12 tumour types in 230 patients from baseline DCE-MRI datasets accumulated from previously completed clinical imaging trials, to enable direct comparison of individual tumours and tumour types. The resulting reference data set was analysed for inter-disease, intra-patient, and intra-tumour heterogeneity in vascular endothelial permeability-driven contrast agent accumulation. This DCE-MRI-based analysis aimed to provide insight into the variation in perfusion and permeability across a broad patient and tumour population.

2. Materials and methods

2.1. Data sets

We accessed a databank of quantitative DCE-MRI studies conducted in our centre over 15 years, largely for the evaluation of putative therapeutic treatments. A single baseline scan from each eligible patient (Fig. 1) in this databank acquired up to May 2013 was analysed in this study using the same software and workflow throughout. Ethical approval was given by the Proportionate Review Sub-Committee of the NRES Committee South Central Berkshire for reanalysis of the data, and informed consent had been provided by the patients. Patients had undergone DCE-MRI with measurements made before, during and after bolus injection of a standard dose (0.1 mmol/kg) of either gadodiamide (Omniscan, GEHC) or gadoterate (Dotarem, Guerbet) via the antecubital vein using a Medrad Spectris power injector (Bayer AG) at a rate of 3 ml/s followed by an equal volume saline flush, also at 3 ml/s. Inclusion criteria for this study were: a consistent data acquisition protocol (a 3D fast field echo protocol with baseline T_1 quantification data acquired using a range of flip angles, and a dynamic acquisition using a constant flip angle); acceptable data acquisition quality; and approval by the original study sponsor. Similar scanning protocols were chosen to allow meaningful direct comparison of the resulting biomarkers, see [15–22] and Table 1.

2.2. Patient characteristics

A total of 230 patients had tumour data suitable for analysis. 45% were male. Median weight was 73 kg (range 44–120). Median age was 62 (range 26–81). The patient cohort contained 342 imaged tumours (with a range of 1 to 7 tumours per patient). Table 2 shows the number of tumours classified by type, as well as the number of patients with that tumour type. A breakdown of patient ages, weights and tumour volumes is shown in Supplementary material.

Just over half (54%) of the imaged tumours were from patients with colorectal primaries. A further 21% were from patients with ovarian primaries. Patients with gliomas and prostate primaries formed the next largest groups of 10% and 5% of tumours respectively.

2.3. DCE-MRI analysis

The data were analysed using in-house analysis software. To ensure comparability of data across studies, all the datasets were analysed from the source signal intensity magnitude files following a prespecified set of standard procedures. All datasets were reviewed to verify that the source data had been acquired in compliance with the original study protocol, and the data were not motion-corrupted. Delineation of the tumour volume region-of-interest (ROI) was normally performed on anatomical, not DCE, images. All ROIs were drawn by a radiographer trained and experienced in tumour definition in MRI (YW; 15 years' experience). Blinding was obviously impossible, because the anatomic location of the tumour is evident in the image. Where an ROI was already available in the dataset, this was reviewed before inclusion into this study. Where no ROI was present or usable, new ROIs were drawn. The ROI was then formed into a mask volume, which was used for the analysis. Both the ROI and the mask were reviewed during a quality control step, in which a second individual checked the lesion edge was properly defined and no obvious errors (such as missing slices) were present. The mask was also checked to ensure that propagation onto the dynamic data set had worked as expected (i.e. the mask lay over the target lesion and was not corrupted). Whole tumour volume measurements (mm^3) were made for each tumour by summing the volume of the voxels in the region of interest.

Baseline T_1 maps for each patient were calculated voxelwise by Levenberg-Marquardt minimisation across three volumetric acquisitions using a set of flip angles shown in Table 1 and applying the fast field echo equation (Eq. (1)) to solve for T_1 and M_0 [24]. Dynamic MRI signal was converted to voxel-wise contrast agent concentration as a function of time [24–26] assuming a linear relationship between concentration and change in relaxation rate (Eq. (2)), where r_1 is the respective longitudinal relaxivity: 3.6 $s^{-1}{\cdot}mM^{-1}$ for gadoterate at 1.5 T; 4.3 $s^{-1}{\cdot}mM^{-1}$ for gadodiamide at 1.5 T; or 4.0 $s^{-1}{\cdot}mM^{-1}$ for gadodiamide at 3 T [27].

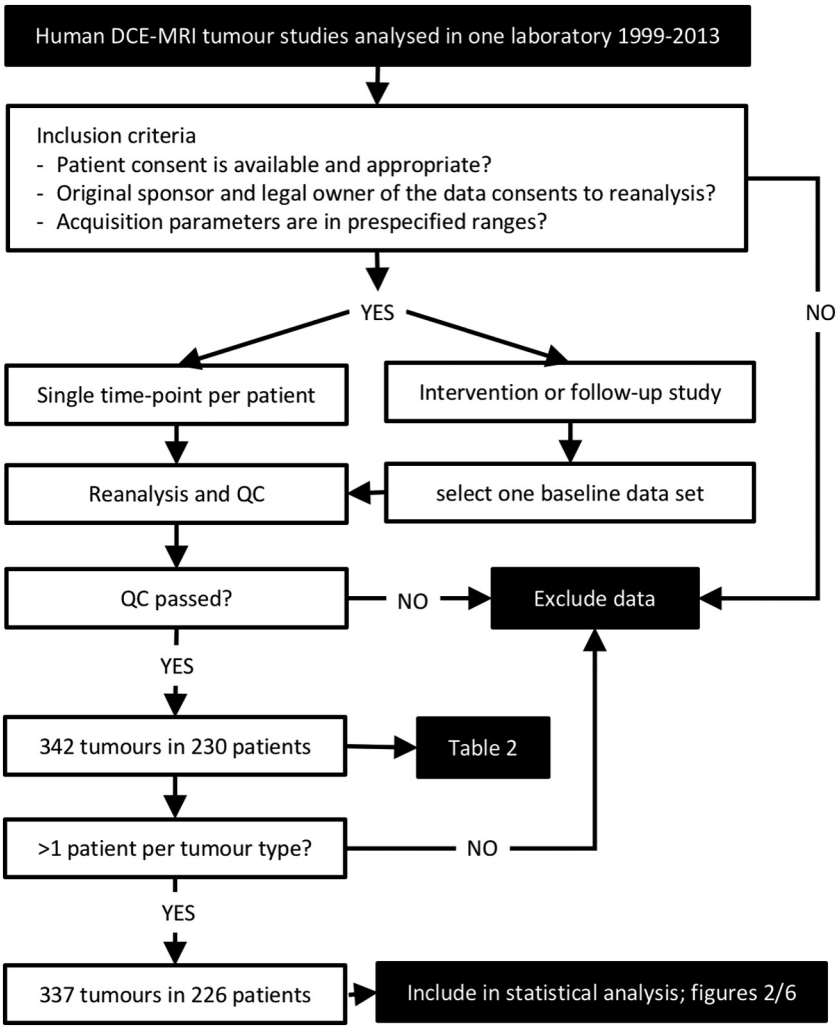

Fig. 1. Flowchart of selection for inclusion in this analysis.

$$S = M_0 \sin\alpha \frac{1 - e^{-TR/T_1}}{1 - \cos\alpha \bullet e^{-TR/T_1}} \quad (1)$$

$$r_1 \times C(t) = \frac{1}{T_1(t)} - \frac{1}{T_0(t)} \quad (2)$$

A population-derived vascular input function was used for each patient to maximise precision [23]. These were used as input in calculations of the extended Kety model [10] (Eq. (3)):

$$C_t(t) = v_p C_p(t) + K^{trans} \int_0^t C_p(t') e^{-\frac{K^{trans}(t-t')}{v_e}} dt' \quad (3)$$

which yields three DCE-MRI parameters:

- K^{trans}, with dimensions min^{-1} and taking any non-negative value, is the volume transfer constant from blood plasma to the extravascular extracellular space and therefore incorporates both perfusion to the tissue and the permeability-surface area product describing transfer across the vascular endothelium.
- v_p (dimensionless, $1 \geq v_p \geq 0$) is the volume fraction which is blood plasma.
- v_e (dimensionless, $1 \geq v_e \geq 0$) is the volume fraction which is extravascular extracellular space.

These three parameters were extracted for each voxel within the regions of interest which demonstrated positive contrast agent accumulation within 60 s of contrast agent arrival to the tumour [28]. The compartmental model assumes that the tumour capillary blood plasma and the extravascular extracellular space are each well-mixed compartments.

2.4. Statistical modelling

Data were classified by tumour type. Where fewer than two patients had a given tumour type, they were excluded from further analysis. Preliminary analyses did not suggest a systematic difference between gadodiamide K^{trans} and gadoterate K^{trans}, so in subsequent modelling K^{trans} differences between the two contrast agents are neglected.

A model of the posterior density of median K^{trans} was built assuming that median K^{trans} values follow a log-normal distribution and fitting a simple Bayesian hierarchical model for median K^{trans}. Formally, if we let y_{ij} be the log of median K^{trans} for subject i, tumour j, then if subject i has tumour type k then $y_{ij} \sim$ Normal (μ_k, σ_k^2); that is, y_{ij} comes from a normal distribution with mean μ_k and variance σ_k^2.

A linear model with tumour type as the only predictor for μ_k was then fitted. That is, if $\underline{x}$ is the covariate matrix with x[i, k] = 1 if subject i has tumour type k and x[i, k] = 0 otherwise and $\boldsymbol{\beta} = (\beta_1 \ldots \beta_K)$ then $\mu_k = \underline{x} \times \boldsymbol{\beta}$.

Weakly–informative priors were chosen as follows: The prior distribution for each β_k was assumed to be Normal (β_0, δ^2), that is, each β_k came from a normal distribution with mean β_0 and variance δ^2. β_0 was drawn from a normal distribution with mean 0 and variance 1000, i.e. $\beta_0 \sim$ Normal (0, 1000), and δ was drawn from the Cauchy distribution centred at 0 with scale parameter equal to 5, i.e. $\delta \sim$ Cauchy (0, 5^2). The prior distribution for σ_k was assumed to be Cauchy centred at 0

Table 1
Protocols used for DCE-MRI data acquisition.

Ref	Scanner	Coil	T_1 map flip angles (deg)	Dynamic flip angle (deg)	TR/TE (ms)	Temporal resolution(s)	Dynamic run length	Voxel size (mm)	Contrast agent
A	Philips Achieva 1.5 T	Q-body	2, 10, 20	20	3/0.82	4.61	130	2.34 × 2.34 × 4	Gadoterate
B	Philips Achieva 1.5 T	XL-Torso	2, 10, 20	20	2.38/0.74	2.95	285	2.34 × 2.34 × 4	Gadoterate
C	Philips Achieva 1.5 T	XL-Torso	2, 8, 15	15	2.34/0.698	3.63	130	2.93 × 2.93 × 3	Gadoterate
D	Philips Achieva 1.5 T	Q-body	2, 10, 20	20	4/0.82	4.97	75	2.93 × 2.93 × 4	Gadoterate
E	Philips Achieva 1.5 T	XL-Torso	2, 10, 20	20	2.34/0.7	1.47	256	2.93 × 2.93 × 3	Gadoterate
F	Philips Achieva 1.5 T	XL-Torso	2, 10, 20	20	2.4/0.74	1.9	256	2.34 × 2.34 × 4	Gadoterate
G	Philips Achieva 1.5 T	Q-body	2, 10, 20	20	4/0.82	4.97	75	2.93 × 2.93 × 4	Gadoterate
H	Philips Achieva 1.5 T	XL-Torso	2, 10, 20	20	2.44/0.8	2.32	155	2.93 × 2.93 × 7	Gadoterate
I	Philips Intera 1.5 T	Q-body	2, 10, 20	20	4/0.82	4.97	75	2.93 × 2.93 × 4	Gadodiamide
J	Philips Intera 1.5 T	Q-body	2, 10, 20	20	4/0.82	4.97	75	3.52 × 3.52 × 4	Gadodiamide
K	Philips Intera 1.5 T	Q-body	2, 10, 20	20	4/0.82	4.97	75	2.93 × 2.93 × 4	Gadoterate
L	Philips Intera 1.5 T	Q-body	2, 10, 20	20	4/0.82	4.97	75	2.93 × 2.93 × 4	Gadodiamide
M	Philips Intera 1.5 T	Q-body	2, 10, 20	20	4/0.82	4.97	75	2.93 × 2.93 × 4	Gadodiamide
N	Philips Intera 1.5 T	Q-body	2, 10, 20	20	4/0.82	4.97	75	2.93 × 2.93 × 4	Gadodiamide
O	Philips Achieva 3 T	SENSE Head-8	2, 10, 16	15	3.5/1.09	3.46	100	1.80 × 1.80 × 2	Gadodiamide
P	Siemens Avanto 1.5 T	Body	5, 10, 25	20	4/0.92	4.2	87	2.93 × 2.93 × 4	Gadodiamide
Q	Philips Intera 1.5 T	Q-body	2, 10, 30	30	4/0.82	4.97	75	2.93 × 2.93 × 4	Gadodiamide
R	GE Signa HDx 1.5 T	8 channel body	2, 10, 20	20	4/1.10	5.04	90	1.46 × 1.46 × 4	Gadoterate

Table 2
Numbers of imaged tumours and patients with primary classification.

Primary cancer	Number of tumours	Number of patients	Protocol reference (number of patients)
Metastatic colorectal	183	93	D (6), G (64), I (1), J (8), K (7), N (1), Q (5), R (1)
Ovarian	71	59	C (10), I (2), K (5), L (9), M (11), N (4), P (15), Q (3)
Glioma	35	34	O (34)
Prostate metastatic to bone	18	13	A (13)
Cervical	7	6	F (3), K (1), N (2)
Renal cell	5	5	H (4), Q (1)
Oesophageal	2	2	E (2)
Gastric	2	1	N (1)
Hepatocellular	4	2	I (1), N (1)
Non-small-cell lung	3	3	R (2), Q (1)
Melanoma	2	2	I (1), R (1)
Primary rectal	2	2	I (2)
Primary endometrial	3	3	K (1), Q (2)
Mesothelioma	1	1	K (1)
Primary prostate	2	2	B (2)
Transitional cell bladder	1	1	I (1)
Primary pancreatic	1	1	K (1)
Total	342	230	230

Protocol reference corresponds to Table 1.

with scale parameter $\sqrt{a_0}$ where $a_0 \sim$ Uniform (0, 65). The upper limit of this Uniform distribution was chosen to be 100 times the maximum median K^{trans} value in the data set.

A Bayesian hierarchical model using Markov Chain Monte Carlo simulation was used to fit the data using JAGS ("Just Another Gibbs Sampler") [http://mcmc-jags.sourceforge.net/] and RJags [http://cran.r-project.org/web/packages/rjags/]. 2000 draws were made from the posterior distribution for each parameter after discarding 1000 draws as burn in. Trace-plots and Gelman plots were used to show convergence. The mean, standard deviation, and 90% quartiles for the posterior distribution of each parameter were calculated.

3. Results

3.1. Variation within disease

To gain insight into tumour permeability, perfusion and accumulation characteristics, two DCE-MRI biomarkers were used: K^{trans} and v_p, as shown in Fig. 2. There was a substantial overlap in the distribution of K^{trans} values across the range of tumours for all tumours other than glioma. Gliomas exhibited the lowest median K^{trans} value of 0.016 min^{-1} and the greatest separation from all other tumour types. The distribution in K^{trans} values for tumour types (excluding glioma) with five or more measures were similar. The median values ranged from 0.10 (cervical) to 0.21 min^{-1} (prostatic metastases). The median values for the tumour types with lower number of samples appeared consistent with the spread of this cohort of tumours (from 0.12 for prostate to 0.25 min^{-1} for endometrial primaries). The geometric mean across all the K^{trans} measurements, excluding gliomas, was 0.15 min^{-1} with a standard deviation in log_e space of 1.76, giving a 95% confidence interval of (0.05 min^{-1}, 0.45 min^{-1}). The gliomas had a geometric mean of 0.015 min^{-1} with a standard deviation in log_e space of 1.07, giving a 95% confidence interval of (0.002 min^{-1}, 0.12 min^{-1}). v_p showed more discrimination between the tumour types, with the renal cell primaries showing the largest median blood plasma space of the tumour types for which more than five measurements were made.

The posterior densities of median K^{trans} for the six most frequently observed tumour types are shown in Fig. 3. These demonstrate that while the expected values of K^{trans} estimated from the data in Fig. 2(a)

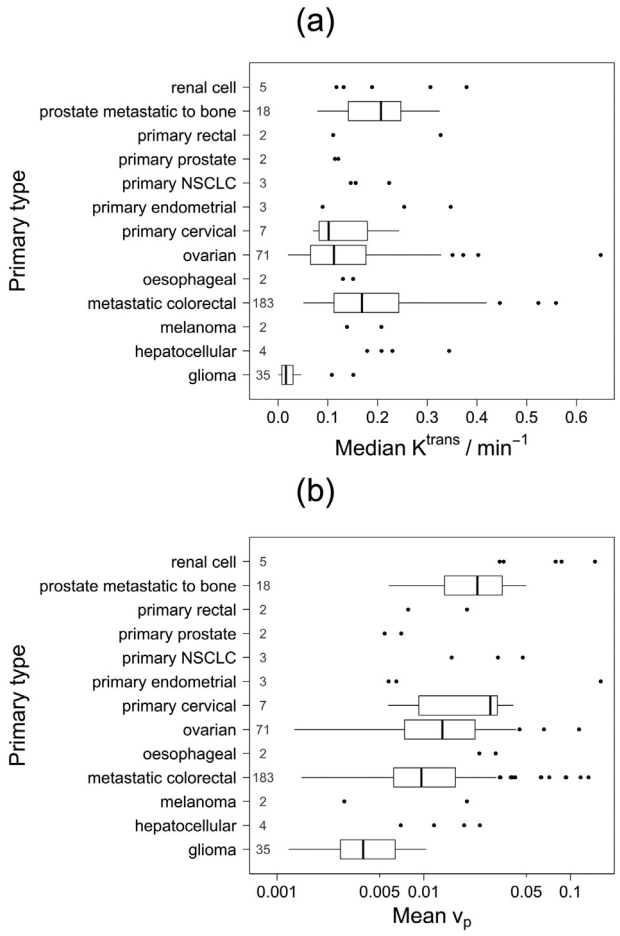

Fig. 2. Mean and range of DCE-MRI parameter values by tumour type for (a) median K^{trans} and (b) mean v_p (log scale). The number of observations is indicated for each tumour type.

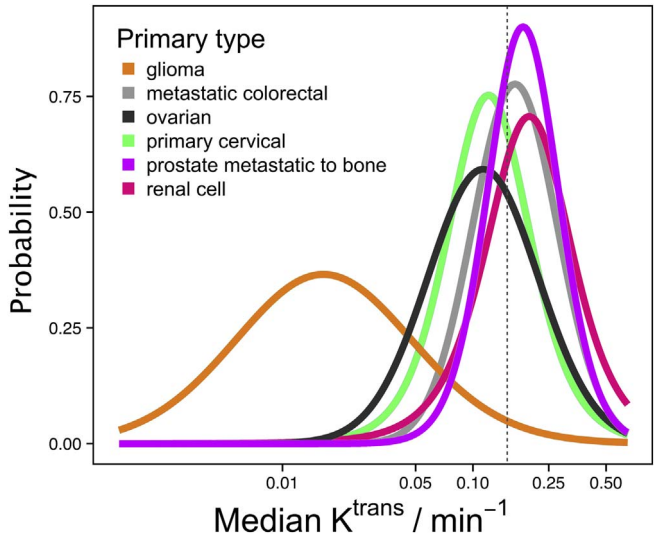

Fig. 3. Posterior density of K^{trans} for primary tumour types glioblastoma multiforme, metastatic colorectal cancer, ovarian, primary endometrial cancer, prostate cancer metastatic to bone and renal cell cancer. The geometric mean of the non-glioma tumours is indicated by the dashed line.

do vary between the tumour types, there is insufficient separation between the posterior densities to be able to predict the K^{trans} value of a tumour given the tumour type, except to say that the median K^{trans} for gliomas are below 0.05 min^{-1} with 80% probability, and median K^{trans}

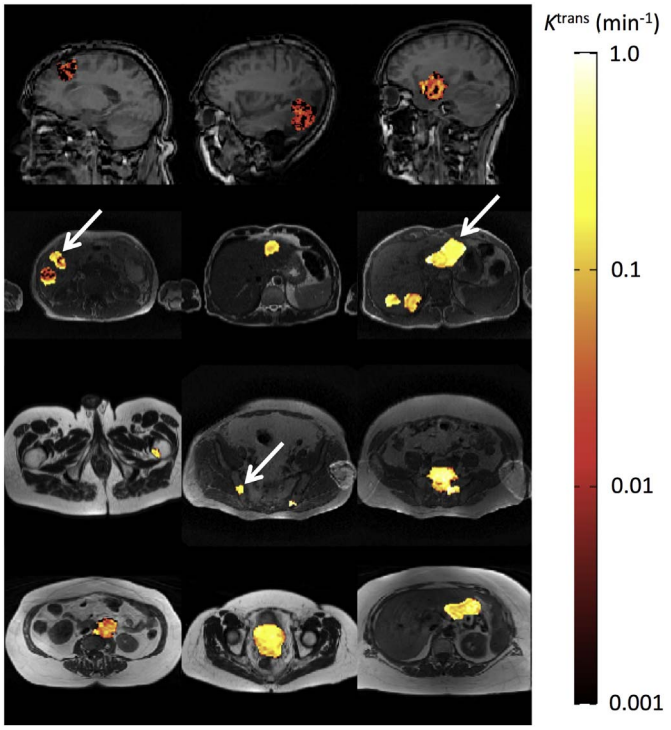

Fig. 4. Example K^{trans} maps overlaid on patient anatomy for patients with median K^{trans} measurements near the (left) lower quartile, (centre) median and (right) upper quartile of the distribution for the primary tumour type. From top to bottom the primary tumour types were: high grade glioma; multiple liver metastases from primary colorectal adenocarcinoma; bone metastases from primary prostatic adenocarcinoma; and stage III/IV ovarian adenocarcinoma with lesions in (left) para-aortic lymph node, (centre) central pelvic mass and (right) a sub-serosal liver metastasis. Where multiple tumours are present, an arrow indicates the tumour with the lower quartile, median or upper quartile measurement.

measurements for the remaining tumour types are between 0.05 and 0.4 min^{-1} with 80% probability.

Because of the possibility that differences in sampling periods (between 6 and 14 min) could bias K^{trans}, we investigated the relationship across all tumours (excluding gliomas) between K^{trans} and sampling period. Essentially no correlation was found (R^2 = 0.00073).

Examples of a series of anatomical MRI images are shown in Fig. 4. These have superimposed K^{trans} parametric maps representing slices from tumours with low, median and high median K^{trans} values (left, middle and right columns respectively) and for the four different primary tumour types: glioma, colorectal, prostate and ovarian. The images illustrate the variability of the transfer constant values within tumour types as well as across tumour types, and highlight the wide range of measurements that can be expected in a patient population.

3.2. Variation within patients

When more than one tumour was present in a patient, the minimum and maximum value of the median transfer constant K^{trans} was obtained for each of those patients and shown in Fig. 5.

3.3. Variation within tumours

Imaging techniques can be used to assess the heterogeneity of contrast agent uptake across an individual tumour lesion [29]. Fig. 6(a) demonstrates that tumours with high median K^{trans} values tend to have a wider range of transfer constant values, which corresponds to higher intra-tumoural heterogeneity. In our data, tumours of primary type colorectal, with high median K^{trans} and high interquartile range, are well separated from those of primary type gliomas with low median

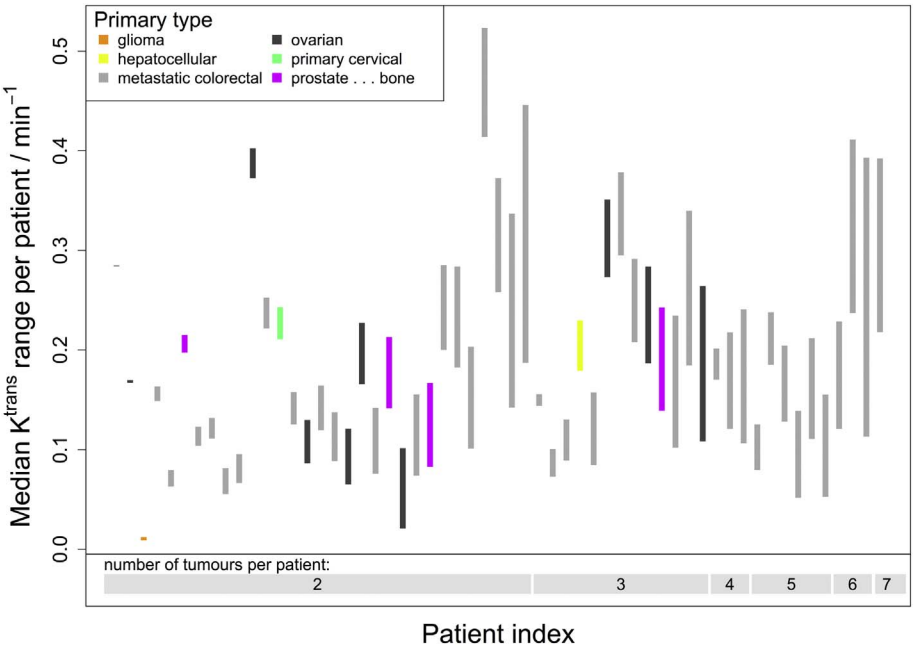

Fig. 5. Intrapatient variability of K^{trans} measurements in terms of the minimum and maximum median K^{trans} values observed for each patient ordered by number of tumours and the range of observations. The number of tumours per patient and tumour type are indicated.

K^{trans} and interquartile range, indicating that the former tumour type presents higher transfer constants (as shown also in Fig. 3) with a wider range than the latter tumour type. Although the dispersion between gliomas and other primary tumour types is clear, there is significant overlap in the scatterplot between the other primary tumour types in a similar manner to that of the median K^{trans} values by primary tumour measurements (Fig. 2(a)).

Variation in K^{trans} between (and, by implication of Fig. 6(a), within) tumours was not related to tumour size (Fig. 6(b)). This plot shows that, while there was a large range in the volumes of most of the tumour types, there was no association between the measured volume and the median K^{trans} measurement for those parts of tumour which demonstrate contrast agent delivery.

4. Discussion

The motivation for this study work arose from current challenges in anticancer drug development. It is often difficult for the drug developer to choose the tumour type(s) in which to undertake trials and seek regulatory approval. For drugs where the Enhanced Permeability and Retention effect is thought to be important, it would be very valuable to know that certain tumour types have a consistently and unusually high K^{trans}, so that the drug developer could initiate clinical trials specifically in those cancers. This critical information is currently missing from the imaging literature and makes personalised medicines and healthcare more challenging, particularly for novel drug delivery products and nanomedicines. The study was based on a convenience sample of patients having tumours from different tissues of origin with a range of different histopathological characteristics (e.g., complex and simple matrix organisation, fibroblast content, vascular localisation and density, etc.), which will affect drug accumulation and retention [7,30–32]. Our convenience set was heavily weighted to local Phase I drug trial populations: precisely the setting in which investigational drugs are likely to be initially evaluated. A major feature of the study is that all 230 patients' data were analysed anew with the same software, algorithms and workflow, and it is this which made possible a direct comparison between diverse tumour types. Our inclusion criteria were designed to avoid extreme variability between the original data acquisition protocols. However, there were minor differences between acquisition protocols among the 18 included studies, and since most of those studies were restricted to a single tumour type, any attempt to account for the variability in data acquisition would be confounded by tumour type.

Our hypothesis was that different tumour types exhibit different K^{trans} reflecting different permeability and perfusion. The gliomas were found to constitute a distinct population, clearly separated from other tumour types. The expectation from the posterior density analysis was that 80% of gliomas would show a K^{trans} value of $< 0.05\ min^{-1}$, and 80% of the remaining tumour types expected to show K^{trans} values between $0.05\ min^{-1}$ and $0.4\ min^{-1}$. Remarkably, after gliomas have been removed from the set, the data provide little or no support for our initial hypothesis. Tumour-to-tumour variability in uptake characteristics was high, and this was plainly evident even for tumour types where as few as two patients were available. Considerable inter-lesion variability was observed within individual patients. Collectively the data imply that, where endothelial permeability affects exposure, selecting patients for treatment based simply on tumour type will not enrich the population for positive therapeutic response. Rather, a patient-specific selection strategy should be adopted, identifying individual lesions with different perfusion and permeability characteristics.

Different tumours within the same patient can have very different permeability and perfusion characteristics. The patients in this sample with multiple tumours had mainly prostate, ovarian and metastatic colorectal cancer. The range of median K^{trans} values tended to increase with the number of tumours. Moreover, many patients showed an intrapatient range similar to the inter-patient range of K^{trans} values [29]. This suggests that effective drug delivery for patients with multiple tumours may be influenced by the characteristics of the individual tumours in the patient, and that different lesions within a single patient may respond differently.

Average K^{trans} within an individual tumour correlated with the range of K^{trans} values measured across the tumour, suggesting an increased intratumoural heterogeneity for tumours with high K^{trans} for those areas of the tumour with contrast agent delivery. A high average K^{trans} does not exclude the possibility of low perfusion/permeability regions. Heterogeneity is a key feature of tumour biology [33] and is highly relevant to drug delivery and tumour pharmacokinetics [34,35]; for example, if high vascular heterogeneity is due to local 'hotspots' then the drug may not achieve a uniform distribution across the tumour [36]. This could mean either limited drug exposure or the potential for a depot effect for a drug that diffuses easily throughout the tumour.

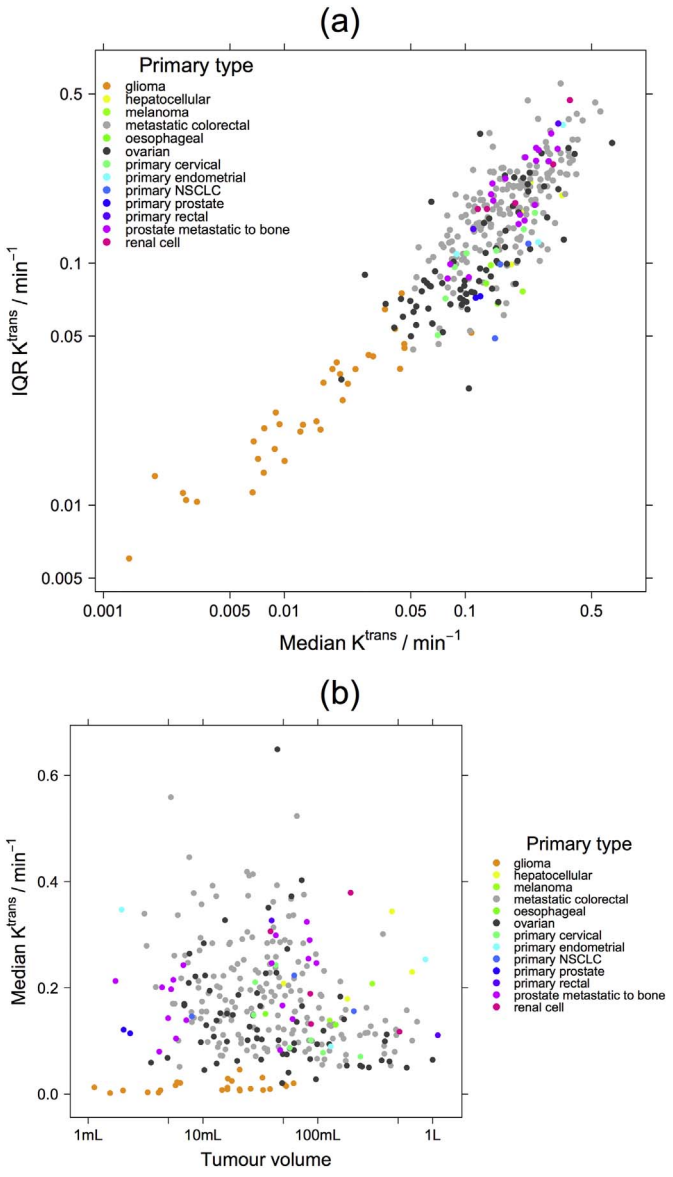

Fig. 6. Scatterplots showing (a) median K^{trans} value versus the interquartile range of K^{trans} values for each tumour investigated, and (b) median K^{trans} values against whole tumour volume.

Heterogeneity was lesion dependent and tumour volume was not predictive of K^{trans}. This further highlights the need to characterise each individual target lesion prospectively in clinical trials.

A limitation of this study is that the contrast agents used were smaller than the drugs and formulations thought to benefit most from enhanced permeability and retention. While convection and enhanced permeability [37,38] to larger molecules or nanoformulations should be reflected in enhanced permeability to contrast agents of < 1 kDa such as gadodiamide or gadoterate, the converse may not be true. Although large-molecule contrast agents such as ferucarbotran or gadomelitol have been used in man, they are now unavailable in most jurisdictions and are therefore unsuitable for a personalised medicine approach.

There is precedent in using an imaging biomarker to provide a companion diagnostic of drug access to tumour. [^{90}Y]-ibritumomab tiuxetan (Zevalin) [39] and [^{131}I]-tositumomab (Bexxar) [40] were each approved by FDA with a predictive SPECT biomarker, while the investigational anticancer agents MM-302 [41] and MM-398 [42] are reportedly in development respectively with PET-based and MRI-based companion diagnostics. Although lack of standardisation of DCE-MRI biomarkers would previously have precluded their use as companion diagnostics, recent initiatives [43,44] now provide a platform for standardisation.

In conclusion, our study shows that for many important tumour types, perfusion and permeability are idiopathic parameters which cannot be predicted but must be measured prospectively in every region of every lesion in every patient.

Supplementary data to this article can be found online at https://doi.org/10.1016/j.mri.2017.11.008.

Conflicts of interest

This work was funded by AstraZeneca, a for-profit company engaged in the discovery, development, manufacturing and marketing of therapeutic pharmaceutical products.

Hervé Barjat and John C. Waterton are former employees of, and shareholders in, AstraZeneca. Mary Jenner is a former employee of AstraZeneca. Jennifer I. Hare, Simon T. Barry, and Sanyogitta Puri are employees of AstraZeneca. Geoffrey J. M. Parker is a director and shareholder of Bioxydyn Limited, a company with an interest in DCE-MRI. Susan Cheung, James PB O'Connor, Yvonne Watson, Ross Little, and Katherine Holliday declare no conflicts of interest.

Acknowledgements

We thank the Christie NHS Foundation Trust, and all the sponsors of the original studies for permitting this reanalysis of their data. This project was supported by researchers at the NIHR Manchester Biomedical Research Centre.

References

[1] European Society of Radiology (ESR). Medical imaging in personalised medicine: a white paper of the research committee of the European Society of Radiology (ESR). Insights Imag 2015;6:141–55.
[2] Matsumura Y, Maeda H. A new concept for macromolecular therapeutics in cancer chemotherapy: mechanism of tumoritropic accumulation of proteins and the antitumor agent smancs. Cancer Res 1986;46:6387–92.
[3] Greish K. Enhanced permeability and retention of macromolecular drugs in solid tumors: a royal gate for targeted anticancer nanomedicines. J Drug Target 2007;15:457–64.
[4] Seymour LW. Passive tumor targeting of soluble macromolecules and drug conjugates. Crit Rev Ther Drug Carrier Syst 1992;9:135–87.
[5] Ekdawi SN, Jaffray DA, Allen C. Nanomedicine and tumor heterogeneity: concept and complex reality. Nano Today 2016;11:402–14.
[6] Taurin S, Nehoff H, Greish K. Anticancer nanomedicine and tumor vascular permeability; where is the missing link? J Control Release 2012;164:265–75.
[7] Prabhakar U, Maeda H, Jain RK, et al. Challenges and key considerations of the enhanced permeability and retention effect for nanomedicine drug delivery in oncology. Cancer Res 2013;73:2412–7.
[8] Harrington KJ, Mohammadtaghi S, Uster PS, et al. Effective targeting of solid tumors in patients with locally advanced cancers by radiolabeled pegylated liposomes. Clin Cancer Res 2001;7:243–54.
[9] Tofts PS, Brix G, Buckley DL, et al. Estimating kinetic parameters from dynamic contrast-enhanced T(1)-weighted MRI of a diffusable tracer: standardized quantities and symbols. J Magn Reson Imaging 1999;10:223–32.
[10] O'Connor JPB, Jackson A, Parker GJM, et al. Dynamic contrast-enhanced MRI in clinical trials of antivascular therapies. Nat Rev Clin Oncol 2012;9:167–77.
[11] Drevs J, Siegert P, Medinger M, et al. Phase I clinical study of AZD2171, an oral vascular endothelial growth factor signaling inhibitor, in patients with advanced solid tumors. J Clin Oncol 2007;25:3045–54.
[12] O'Connor JPB, Jayson GC. Do imaging biomarkers relate to outcome in patients treated with VEGF inhibitors? Clin Cancer Res 2012;18:6588–98.
[13] Huang W, Li X, Chen Y, et al. Variations of dynamic contrast-enhanced magnetic resonance imaging in evaluation of breast cancer therapy response: a multicenter data analysis challenge. Transl Oncol 2014;7:153–66.
[14] O'Connor JPB, Aboagye EO, Adams JE, et al. Imaging biomarker roadmap for cancer studies. Nat Rev Clin Oncol 2017;14:169–86.
[15] Horsley L, Cummings J, Middleton M, et al. A phase 1 trial of intravenous 4-(*N*-(*S*-glutathionylacetyl)amino) phenylarsenoxide (GSAO) in patients with advanced solid tumours. Cancer Chemother Pharmacol 2013;72:1343–52.
[16] Linnik IV, Scott MLJ, Holliday KF, et al. Noninvasive tumor hypoxia measurement using magnetic resonance imaging in murine U87 glioma xenografts and in patients with glioblastoma. Magn Reson Med 2014;71:1854–62.
[17] Mills SJ, Soh C, O'Connor JPB, et al. Tumour enhancing fraction (EnF) in glioma: relationship to tumour grade. Eur Radiol 2009;19:1489–98.

[18] Mitchell CL, O'Connor JPB, Jackson A, et al. Identification of early predictive imaging biomarkers and their relationship to serological angiogenic markers in patients with ovarian cancer with residual disease following cytotoxic therapy. Ann Oncol 2010;21:1982–9.
[19] Mitchell CL, O'Connor JPB, Roberts C, et al. A two-part phase II study of cediranib in patients with advanced solid tumours: the effect of food on single-dose pharmacokinetics and an evaluation of safety, efficacy and imaging pharmacodynamics. Cancer Chemother Pharmacol 2011;68:631–41.
[20] Mullamitha SA, Ton NC, Parker GJM, et al. Phase I evaluation of a fully human anti-v integrin monoclonal antibody (CNTO 95) in patients with advanced solid tumors. Clin Cancer Res 2007;13:2128–35.
[21] O'Connor JPB, Carano RAD, Clamp AR, et al. Quantifying antivascular effects of monoclonal antibodies to vascular endothelial growth factor: insights from imaging. Clin Cancer Res 2009;15:6674–82.
[22] O'Connor JPB, Naish JH, Parker GJM, et al. Preliminary study of oxygen-enhanced longitudinal relaxation in MRI: a potential novel biomarker of oxygenation changes in solid tumors. Int J Radiat Oncol 2009;75:1209–15.
[23] Parker GJM, Roberts C, Macdonald A, et al. Experimentally-derived functional form for a population-averaged high-temporal-resolution arterial input function for dynamic contrast-enhanced MRI. Magn Reson Med 2006;56:993–1000.
[24] Li KL, Zhu XP, Waterton J, Jackson A. Improved 3D quantitative mapping of blood volume and endothelial permeability in brain tumors. J Magn Reson Imaging 2000;12:347–57.
[25] Bernstein MA, King KF, Zhou XJ. Handbook of MRI pulse sequences. Academic Press; 2004.
[26] Stanisz GJ, Henkelman RM. Gd-DTPA relaxivity depends on macromolecular content. Magn Reson Med 2000;44:665–7.
[27] Rohrer M, Bauer H, Mintorovitch J, Requardt M, Weinmann HJ. Comparison of magnetic properties of MRI contrast media solutions at different magnetic field strengths. Investig Radiol 2005;40:715–24.
[28] Evelhoch JL. Key factors in the acquisition of contrast kinetic data for oncology. J Magn Reson Imaging 1999;10:254–9.
[29] O'Connor JPB, Rose CJ, Waterton JC, et al. Imaging intratumor heterogeneity: role in therapy response, resistance, and clinical outcome. Clin Cancer Res 2015;21:249–57.
[30] Bertrand N, Wu J, Xu X, et al. Cancer nanotechnology: the impact of passive and active targeting in the era of modern cancer biology. Adv Drug Deliv Rev 2014;66:2–25.
[31] Miao L, Lin CM, Huang L. Stromal barriers and strategies for the delivery of nanomedicine to desmoplastic tumors. J Control Release 2015;219:192–204.
[32] Song G, Darr DB, Santos CM, et al. Effects of tumor microenvironment heterogeneity on nanoparticle disposition and efficacy in breast cancer tumor models. Clin Cancer Res 2014;20:6083–95.
[33] Junttila MR, de Sauvage FJ. Influence of tumour micro-environment heterogeneity on therapeutic response. Nature 2013;501:346–54.
[34] Denison TA, Bae YH. Tumor heterogeneity and its implication for drug delivery. J Control Release 2012;164:187–91.
[35] Hansen AE, Petersen AL, Henriksen JR, et al. Positron emission tomography based elucidation of the enhanced permeability and retention effect in dogs with cancer using Copper-64 liposomes. ACS Nano 2015;9:6985–95.
[36] Ekdawi SN, Stewart JMP, Dunne M, et al. Spatial and temporal mapping of heterogeneity in liposome uptake and microvascular distribution in an orthotopic tumor xenograft model. J Control Release 2015;207:101–11.
[37] Stapleton S, Allen C, Pintilie M, Jaffray DA. Tumor perfusion imaging predicts the intra-tumoral accumulation of liposomes. J Control Release 2013;172:351–7.
[38] Butowski N, Bankiewicz K, Kells A, et al. A phase I study of convection-enhanced delivery of liposomal-irinotecan using real-time imaging with gadolinium in patients with recurrent high grade glioma. Neuro-Oncology 2014;16(Suppl 3):iii13.
[39] US Food & Drug Administration. Biologic License Application 125019 ZEVALIN (IBRITUMOMAB TIUXETAN): original label. http://www.accessdata.fda.gov/drugsatfda_docs/label/2002/ibriide021902LB.pdf; 2002, Accessed date: 1 November 2017.
[40] US Food & Drug Administration. Biologic License Application 125011 BEXXAR (TOSITUMOMAB; IODINE I 131 TOSITUMOMAB): original label. http://www.accessdata.fda.gov/drugsatfda_docs/label/2003/tosicor062703LB.pdf; 2003, Accessed date: 1 November 2017.
[41] Merrimack Pharmaceuticals. [64Cu]-Labeled Brain PET/MRI for MM-302 in Advanced HER2 + Cancers With Brain Mets Available via https://clinicaltrials.gov/ct2/show/NCT02735798; 2016, Accessed date: 30 November 2016.
[42] Kalra AV, Spernyak J, Kim J, et al. Abstract 2065: magnetic resonance imaging with an iron oxide nanoparticle demonstrates the preclinical feasibility of predicting intratumoral uptake and activity of MM-398, a nanoliposomal irinotecan (nal-IRI). Cancer Res 2014;74(19 Supplement):2065.
[43] Leach MO, Morgan B, Tofts PS, et al. Imaging vascular function for early stage clinical trials using dynamic contrast-enhanced magnetic resonance imaging. Eur Radiol 2012;22:1451–64.
[44] DCE MRI Technical Committee. DCE MRI Quantification Profile, Quantitative Imaging Biomarkers Alliance. Version 1.0. Reviewed Draft. QIBA July 1, 2012 Available via http://rsna.org/QIBA_.aspx, Accessed date: 31 January 2017.